Available online at www.sciencedirect.com
ScienceDirect
Journal of Sound and Vibration 306 (2007) 419–443
JOURNAL OF SOUND AND VIBRATION
www.elsevier.com/locate/jsvi

"Buzz-saw" noise: A comparison of modal measurements with an improved prediction method

A. McAlpine[a,*], M.J. Fisher[a], B.J. Tester[b,1]

[a]Institute of Sound and Vibration Research, University of Southampton, Highfield, Southampton S017 1BJ, UK
[b]Rolls-Royce plc, Derby, P.O. Box 31, DE24 8BJ, UK

Received 26 September 2005; received in revised form 29 November 2006; accepted 23 April 2007

Abstract

"Buzz-saw" noise is radiated from a turbofan inlet duct when the fan tip speed is supersonic. In a recent article the effect of an acoustic liner on buzz-saw noise has been examined. Spectral measurements in a rigid and an acoustically lined inlet duct have been compared. Also these measurements have been utilized to assess a buzz-saw noise prediction method. The prediction method is based on a one-dimensional nonlinear propagation model. Sound absorption by an acoustic lining can be included in the model. In this article, the buzz-saw noise prediction method is improved by the inclusion in the modelling of the effect of a boundary layer on absorption of sound in a lined duct. Also, modal measurements from a circumferential microphone array have been examined. These show that the principal source of buzz-saw noise is not always the rotor-alone pressure field. Non-rotor-alone scattered tones can be a significant source of buzz-saw noise at low supersonic fan speeds. The numerical simulations, which only predict the rotor-alone tones, have been re-evaluated in light of these new modal measurements.

1. Introduction

"Buzz-saw" noise is the principal fan tone noise source radiated from a turbofan inlet duct at supersonic fan speeds. The noise source consists of a set of tones, known as engine orders (EO) that are harmonics of the engine's shaft rotation frequency. These EO tones are the buzz-saw noise.

Accurate prediction of buzz-saw noise is a challenging problem in computational aeroacoustics because the analysis will involve nonlinear acoustics, modelling a complete fan blade set (i.e. a full three-dimensional geometry), modelling an acoustic liner and calculations at high frequencies.

A recent series of papers has described new work concerning the application of one-dimensional nonlinear propagation models to predict buzz-saw noise, see Refs. [1–4]. A numerical simulation model, termed the frequency domain numerical solution or FDNS, has been developed. This is used to calculate the nonlinear propagation of the "rotor-alone" pressure field in either a rigid or an acoustically lined inlet duct.

*Corresponding author. Tel.: +44 23 8059 2667; fax: +44 23 8059 3190.
E-mail address: am@isvr.soton.ac.uk (A. McAlpine).
[1]Present address: Institute of Sound and Vibration Research, University of Southampton, Southampton S017 1BJ, UK.

0022-460X/$ - see front matter © 2007 Elsevier Ltd. All rights reserved.
doi:10.1016/j.jsv.2007.04.053

At supersonic fan speeds, the pressure field that is locked to the rotor, i.e. the steady rotor-alone field in the rotor's frame of reference, propagates upstream against the oncoming flow.[2] The acoustic signature of this pressure field is a set of EO tones, known as the rotor-alone EO tones. The simulation model is used to predict the nonlinear propagation of the rotor-alone pressure field inside an inlet duct. From this the level of the rotor-alone EO tones can be determined. This model can be used for prediction of buzz-saw noise, because it is assumed that the rotor-alone EO tones are the principal component of buzz-saw noise.

In Ref. [2] there is a description of the controlling mechanisms that lead to the generation of buzz-saw noise. This is outlined in terms of a one-dimensional sawtooth pressure waveform that can be used to approximate the rotor-alone pressure field. It is this approximation that enables a one-dimensional nonlinear propagation equation to be utilized: in this case a modified version of Burgers equation. Nonlinear propagation of the rotor-alone pressure field leads to the characteristic buzz-saw noise signature of a supersonic ducted fan.

The key step in the prediction scheme is that the problem is transformed from the time to the modal/frequency domain. Burgers equation (in the frequency domain) is modified by the addition of a linear absorption term. This enables to a first approximation the frequency-dependent absorption properties of an acoustic liner to be included, whilst modelling the nonlinear propagation of the rotor-alone pressure field.

The rotor-alone pressure field is expressed in terms of spinning modes that are all steady in the rotor's frame of reference. These modes have azimuthal mode order $m = \mathrm{EO}$, and are referred to as the rotor-alone EO modes. The absorption properties of the acoustic lining are calculated by using duct acoustics theory. Modes are calculated for a cylindrical acoustically lined duct containing a uniform mean flow, by solving the convected Helmholtz equation. An eigenvalue problem is formulated in order to calculate the axial wavenumbers, k_z, of the modes. From this the decay rates, $\mathrm{Im}\{k_z\}$, of the least attenuated modes are found, which are used in the numerical simulation.

A full outline of the FDNS prediction method is in Refs. [2,3]. These references also contain a review of earlier research on buzz-saw noise. The method was developed primarily to be used for the prediction of buzz-saw noise in lined inlet ducts. In Ref. [2] there are some examples of noise predictions compared with experimental measurements, but only for a rigid inlet duct, because at this time in-duct measurements from a lined duct were not available.

During the recent European Community X-noise research project RESOUND (*Reduction of engine source noise through understanding and novel design*), coordinated by Rolls–Royce, noise measurements were acquired from a model fan rig. New measurements of buzz-saw noise have been obtained in both a rigid and a lined inlet duct. In a recent article, these measurements have been utilized to examine the effect of an acoustic liner on buzz-saw noise, see Ref. [4]. This article is a continuation of that work.

The Rolls–Royce RESOUND model fan rig is shown sketched in Fig. 1. The fan has $B = 26$ fan blades, so BPF is $\mathrm{EO} = B = 26$. Both the rigid and the lined inlet duct contained four microphones, (Kulite pressure transducers), that measured the pressure at the duct wall. In Ref. [4], measurements obtained close to the fan, at Kulite 1, are used to initiate the numerical simulations. Then, the measured and predicted EO frequency spectrum at Kulite 4 are compared. In Ref. [4], there are comparisons between measurement and prediction of buzz-saw noise in the rigid and the lined inlet duct. Results are shown for a range of supersonic fan speeds, referred to as cases A–G, that are listed in this article in Table 1. To the authors' knowledge, this is the first time that these type of buzz-saw noise measurements and numerical predictions in a lined inlet duct have been published. In this article, these experimental results are again utilized.

Figs. 2 and 3 are examples of results from Ref. [4]. With the rigid inlet duct, at each fan speed the EO frequency spectrum is reasonably well predicted by the numerical simulations (see Fig. 2). In particular, the effect of cut-off (low-order EOs only) is captured by the prediction method. The main difference between the measurements and the predictions is seen at high-order EOs at high supersonic fan speeds; for example, see Fig. 2(c, d). This type of discrepancy between the results only occurs at high frequencies. So in Ref. [4] it is suggested that boundary-layer "shielding", that is refraction of sound by the boundary layer, could affect wall measurements at high frequencies.

Another possibility, also discussed in [4], is that at high supersonic fan speeds three-dimensional effects could be significant. The numerical simulations utilize an approximate one-dimensional model of the

[2]At subsonic fan speeds, the rotor-alone pressure field is cut-off.

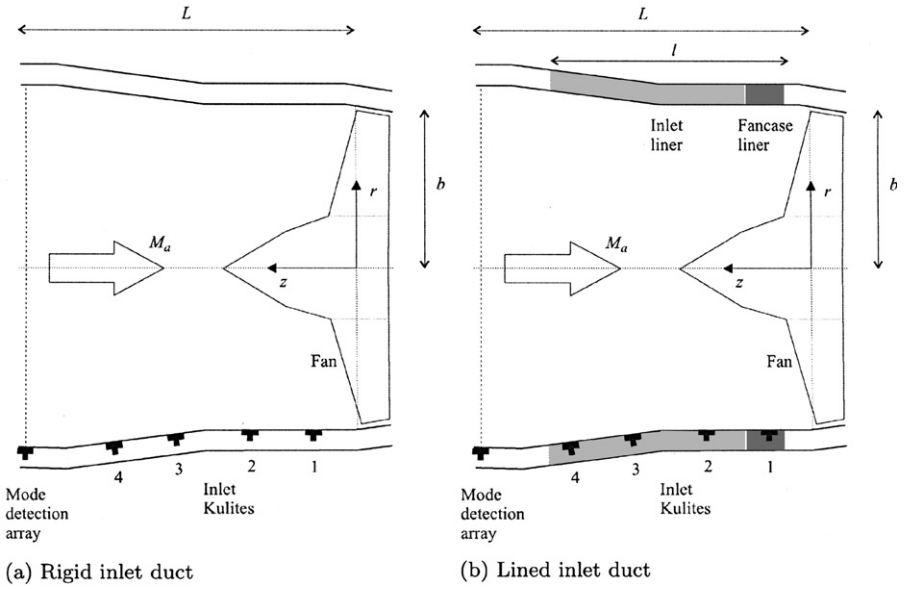

Fig. 1. Sketch of the Rolls–Royce RESOUND model fan rig and inlet duct (not to scale).

Table 1
Rolls–Royce RESOUND Datum fan—supersonic fan speed test cases A–G

Case	Fan speed (%)	M_t	M_a	M_{rel}	BPF (Hz)	kb
A	75	1.03	0.41	1.11	3331	26.8
B	78	1.07	0.43	1.15	3457	27.8
C	81	1.10	0.45	1.19	3565	28.7
D	83	1.14	0.47	1.23	3682	29.6
E	86	1.18	0.49	1.28	3805	30.6
F	89	1.21	0.51	1.31	3911	31.5
G	91	1.24	0.53	1.35	4012	32.2

rotor-alone pressure field. In terms of spinning modes, it is assumed that the pressure field can be modelled by modes (m, 1) with $m = \text{EO}$, i.e. only the first radial mode orders. At high supersonic fan speeds, more higher radial mode orders will be cut-on. Any interference effects between different radial mode orders cannot be modelled using the FDNS. It is known that on approaching the fan's design speed the shocks are swallowed, and the numerical method is no longer valid to be used when this happens.

With the lined inlet duct, in contrast to the results with the rigid duct, there are some significant differences between the measured and predicted EO frequency spectrum at each fan speed (see Fig. 3). These predictions utilize the modal decay rates of the least attenuated EO modes in a lined duct. These are shown in Fig. 4, where the least attenuated mode transmission loss, $\Delta_{\text{LAM}} = -20\,\text{Im}\{k_z\}\log_{10}e$ per unit length, at EO = 1–4B, is plotted for each fan speed case in Fig. 3.

At low supersonic fan speeds, the predicted modal decay rates are high because the rotor-alone EO modes are near cut-off, e.g. Case A, Fig. 4(a). Case A is the lowest supersonic fan speed that is examined. The comparison between measurement and prediction for case A is poor, see Fig. 3(a). However, at higher supersonic fan speeds the EO frequency spectrum is somewhat better predicted by the numerical simulations, see Fig. 3(b–d). Generally, at each fan speed, the simulations under predict the levels of the EO tones at frequencies close to the liner's optimum frequency. At these EOs, more attenuation is predicted than is measured in practice. In Ref. [4] it is suggested that more realistic modal decay rates could be determined by the inclusion of a boundary layer in the modelling. This is because in an inlet duct the sound propagates against the mean flow, and a boundary layer will refract the sound away from the acoustic liner at the duct wall.

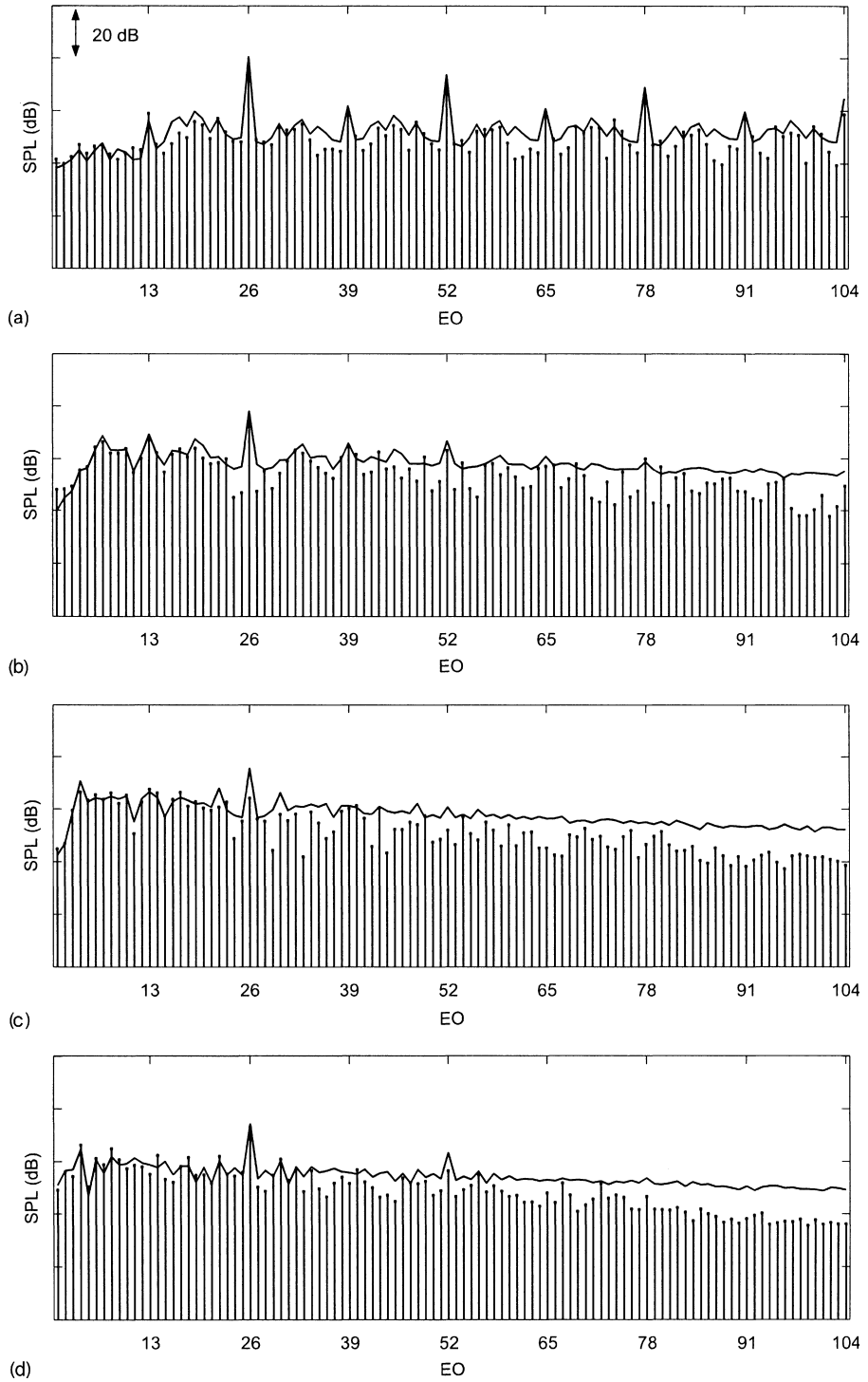

Fig. 2. Measured EO frequency spectrum at Kulite 4 in the rigid inlet duct: (a) Case A; (b) Case C; (c) Case E; and (d) Case G. The FDNS prediction is shown by the solid line. Reproduced from Ref. [4].

The discrepancy noted previously at high frequencies between the measurements and the predictions in the rigid duct, which could be due to boundary-layer shielding, is not seen in the same cases with the lined duct, (compare Figs. 2(c, d) and 3(c, d)). However, measurements in both rigid and lined inlet ducts, at high

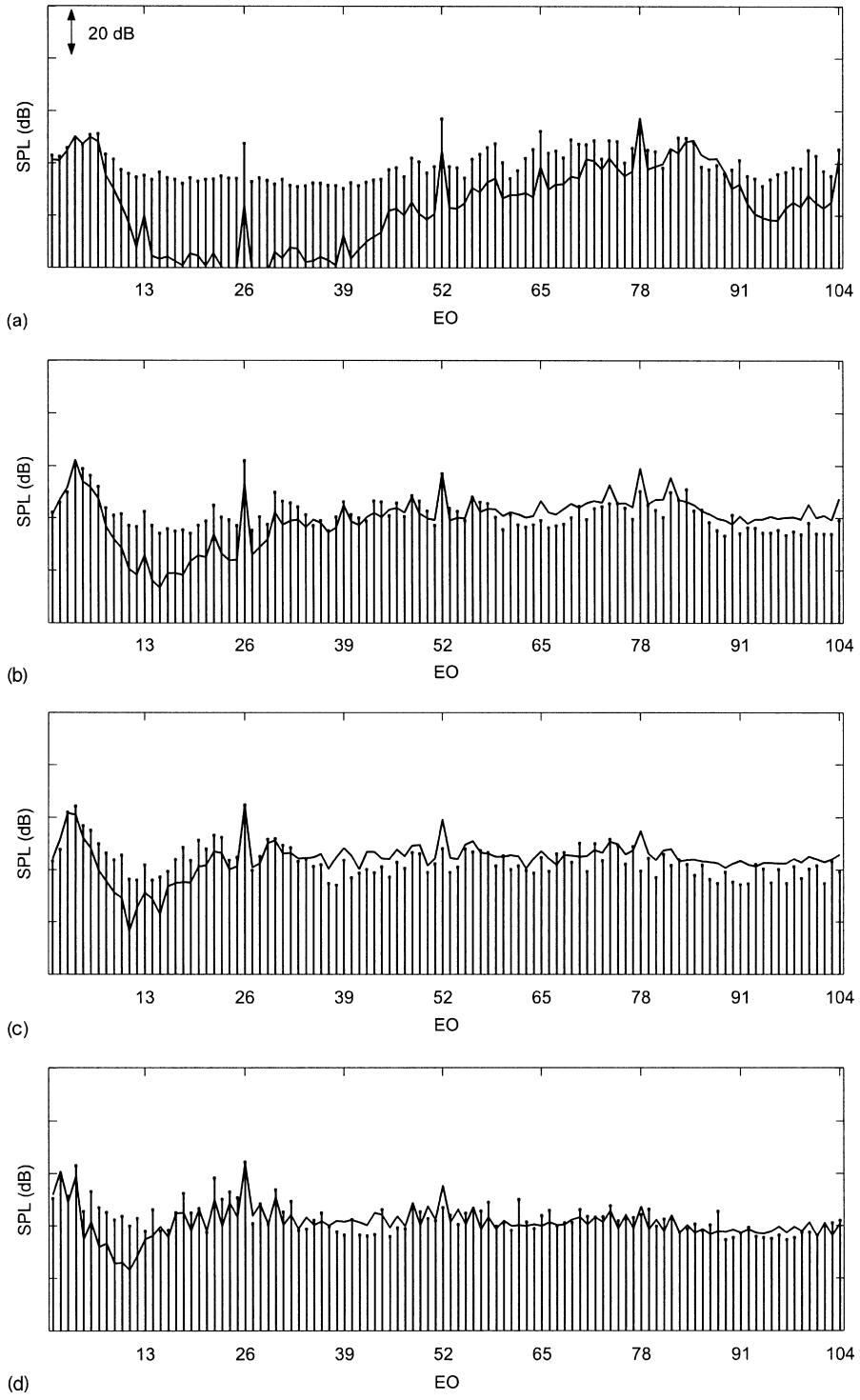

Fig. 3. Measured EO frequency spectrum at Kulite 4 in the lined inlet duct: (a) Case A; (b) Case C; (c) Case E; and (d) Case G. The FDNS prediction is shown by the solid line (uniform flow). Reproduced from Ref. [4].

frequencies, could be affected by shielding. In Ref. [4] it is postulated that the absence of this type of discrepancy between measurement and prediction in the lined duct is misleading, owing to the values of the modal decay rates that are calculated at high frequencies with uniform mean flow. At high frequencies, the

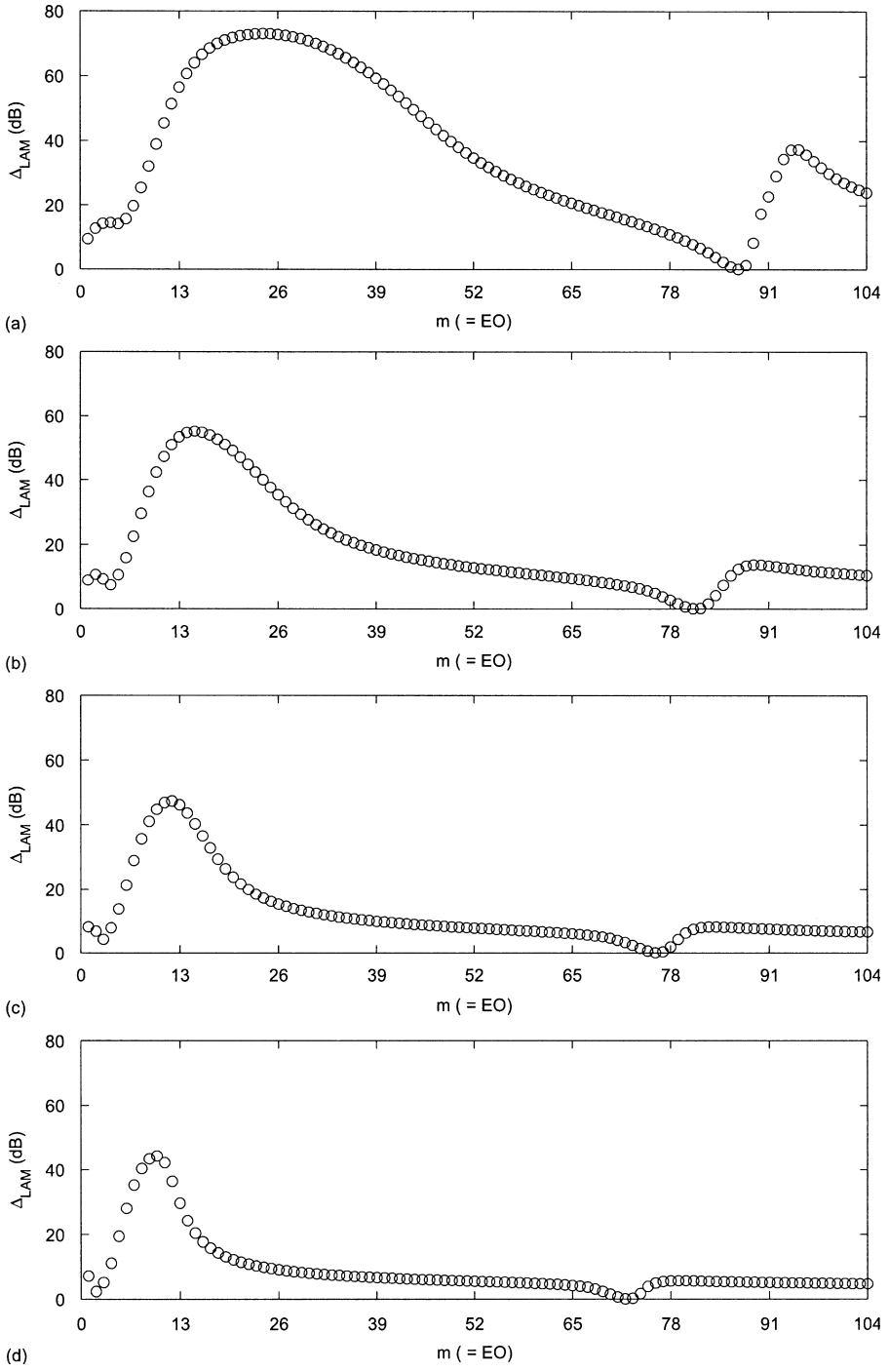

Fig. 4. Predicted attenuation of rotor-alone EO modes (uniform flow). Δ_{LAM} for $m = \mathrm{EO} = 1$ to $4B$: (a) Case A; (b) Case C; (c) Case E; and (d) Case G. Reproduced from Ref. [4].

least attenuated mode transmission losses are predicted to be typically between 5 and 10 dB, e.g. see Fig. 4. The inclusion, at high frequencies, of this small amount of absorption in the numerical simulations, is the reason for the apparent improvement in the predictions with the lined duct compared with the rigid duct. However, owing to the boundary layer, it is questionable whether at high frequencies this absorption does occur in a lined inlet duct.

Therefore, in this article, one of the objectives is to examine the effect of a boundary layer on these buzz-saw noise predictions. The effect of the boundary layer is included in the modelling indirectly, via the use of modified modal decay rates, which are determined based on a mean flow profile that includes a boundary layer. This means that only lined duct noise predictions will be re-calculated using these modified modal decay rates, since in the rigid duct the modal decay rates are all zero (other than for a small number of low-order cut-off modes). Therefore, only the effect of a boundary layer on liner absorption can be quantified in the numerical simulations. The effect of a turbulent boundary layer on the wall measurements is discussed further in Section 3, and how this could affect the comparison between measurement and prediction presented in Ref. [4] and here.

Also, in this article, the second objective is to examine other possible sources of buzz-saw noise. In Ref. [4] it is also postulated that, in particular at low supersonic fan speeds, discrepancies between the measurements and the predictions in the lined inlet duct could be due to non-rotor-alone EO tones generated by scattering. For example, owing to interactions between the steady rotor-alone pressure field, and steady distortion in the mean flow or acoustically "hard" liner splices. These interaction tones can be identified, because they will be unsteady in the rotor's frame of reference, i.e. their azimuthal mode order $m \neq \mathrm{EO}$. It has been assumed previously that the contribution to buzz-saw noise from interaction tones is small. Based on this, the FDNS has been used to predict buzz-saw noise, although strictly it only can be used to predict the rotor-alone EO tones.

In this article, also modal measurements from a circumferential microphone array, located at the end of the inlet duct, are examined. The mode detection array used in the Rolls–Royce model fan rig tests was developed at the National Aerospace Laboratory NLR, The Netherlands. The array consists of 100 wall-mounted microphones arranged in a sparse configuration around the inlet duct. The array was located in the rigid section of the duct, upstream of the acoustic liner. The modal spectrum up to $m = 78$ was measured by using this array (i.e. frequencies up to 3 BPF). The array provides an azimuthal mode breakdown of the sound field, but not radial mode amplitudes. The mode detection technique and some of the results included in this paper are in Ref. [5]. Additional measurements to those in Ref. [5] also have been included in this article.

Analysis of measurements from the mode detection array permit the EO tones to be separated into their rotor-alone and non-rotor-alone components. The numerical simulations only predict the rotor-alone component of the EO tones. In this article the spectral results are re-evaluated by examining the measured levels of the rotor-alone component of each EO tone. It is shown that, at low supersonic fan speeds, there is a significant contribution to the buzz-saw noise from non-rotor-alone sources (predominantly due to scattering caused by the liner splices). This is another reason why there is poor agreement between the measured and predicted EO frequency spectrum at low supersonic fan speeds.

In summary, in this article the type of comparisons between measurement and prediction of buzz-saw noise, first published in Ref. [4], are examined in more detail. The following two items are considered: (1) the effect of a boundary-layer on modal decay rates, and "shielding" at high frequencies—Sections 2 and 3; (2) the effect of non-rotor-alone noise sources—Section 4. Finally, in Section 5 conclusions from this study of buzz-saw noise are discussed, and suggestions for future work are outlined.

2. Sound propagation in a lined duct containing a shear flow

Sound attenuation in a lined flow duct will be affected by the presence of a boundary layer at the duct wall. Simple ray acoustics can be used to demonstrate that a boundary layer will refract upstream sound propagation away from the duct wall. In terms of spinning duct modes, it is anticipated that the modal decay rates will be less when a boundary layer is included in the mean flow profile, compared with a uniform "plug" flow which is an approximation that permits slip at the duct walls.

Several authors in the 1970s considered the effect of a boundary layer on sound propagation in a lined flow duct. The technique used in this work is based on the method developed by Mungur and Plumblee [6], and Eversman [7]. Also see the duct acoustics review article by Eversman [8] in 1991.

For a cylindrical duct containing a uniform axial flow M_a, it is well known that on assuming a harmonic acoustic pressure field $p(r, \theta, z, t) = \hat{p}(r, \theta, z) \exp(\mathrm{i}\omega t)$, solutions of the convected Helmholtz equation can be

expressed in terms of Fourier–Bessel modes

$$\hat{p}_{m,n}(r,\theta,z) = A_{m,n}J_m(\kappa_{m,n}r)e^{i(-k_{zm,n}z\pm m\theta)}, \tag{1}$$

where $A_{m,n}$ is a constant and J_m is the Bessel function of the first kind of order m. The modes have azimuthal and axial wavenumber m and $k_{zm,n}$ respectively. The radial wavenumbers $\kappa_{m,n}$ also are known as the radial eigenvalues because they are found by solving an eigenvalue problem that is formulated by combining Eq. (1) with the duct wall boundary condition.

Similarly, with a sheared mean-flow profile $M = M(r)$ there exist harmonic modal solutions of the form

$$\hat{p}_{m,n}(r,\theta,z) = P_{m,n}(r)e^{i(-k_{zm,n}z\pm m\theta)}, \tag{2}$$

where the sheared flow model equation for $P(r)$ satisfies the ordinary differential equation

$$\frac{d^2P}{dr^2} + \left[\frac{1}{r} + \frac{2k_{zm,n}/k}{1 - Mk_{zm,n}/k}\frac{dM}{dr}\right]\frac{dP}{dr} + \left[(k - Mk_{zm,n})^2 - (k_{zm,n})^2 - \frac{m^2}{r^2}\right]P = 0 \tag{3}$$

in the case of uniform fluid density ρ_0 and sound speed c_0, and $k = \omega/c_0$. Pridmore-Brown [9] derived the two-dimensional version of Eq. (3). This equation is also the compressible version of the well-known Rayleigh equation in hydrodynamic stability.

With a uniform flow, the duct modes are identified by their azimuthal and radial order (m, n). (In a rigid duct the boundary condition reduces to simply $J'_m(\kappa_{m,n}b) = 0$, and the radial eigenvalue $\kappa_{m,n}$ denotes the nth turning point of the Bessel function J_m.) With a 'thin' boundary-layer profile it is anticipated that the mode shapes will be similar to the modes with a uniform flow, at least in the region outside the boundary layer. Therefore, in this article the duct modes calculated with a boundary-layer flow also are identified by azimuthal and radial order (m, n). The radial order n associates this mode with its corresponding uniform-flow mode.

Most calculations of this type in Refs. [6,7] were at non-dimensional frequency, or Helmholtz number, kb up to about 10. However, the buzz-saw numerical simulations include rotor-alone EO modes at frequencies up to 10 BPF, with azimuthal mode order $m = \mathrm{EO} = 10B$. This is equivalent to kb between about 250 and 300 (depending on the fan speed). The computational frequency range includes very high frequencies to ensure good resolution of the sawtooth pressure waveform that approximates the rotor-alone pressure field. At these high frequencies it is anticipated that the boundary-layer will completely "shield" the sound from the duct wall, because the acoustic wavelength will be comparable with the boundary-layer thickness. The numerical method in Refs. [6,7] has been modified in order to be used at high frequencies.

The mean velocity profile $M(r)$ in an aero-engine inlet duct is assumed to closely resemble a 1/5th power law boundary layer. The boundary-layer thickness δ is assumed to be 4% of the duct radius b.[3] Therefore,

$$M(r) = M_a, \quad 0 \leqslant r \leqslant b(1-\delta), \tag{4}$$

$$= M_a\left(\frac{1-(r/b)}{\delta}\right)^{1/5}, \quad b(1-\delta) \leqslant r \leqslant b. \tag{5}$$

The boundary-layer profile is sketched in Fig. 5.

At $r = b$ the duct wall boundary condition is

$$\frac{dP}{dr} = f_b(k_z)P, \tag{6}$$

where

$$f_b = -ikA\left(1 - M\frac{k_z}{k}\right)^2 \tag{7}$$

and A is the non-dimensional specific acoustic admittance of the liner.

[3]These values were used following consultation with Rolls–Royce.

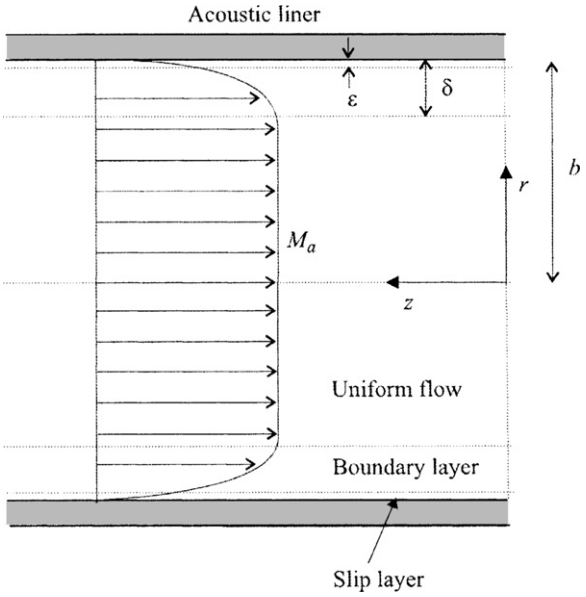

Fig. 5. Boundary-layer flow.

At $r = b$ there is no slip ($M = 0$), but $\mathrm{d}M/\mathrm{d}r$ is singular as $r \to b$, so the boundary condition is applied a small distance ε from the duct wall where $M \neq 0$. The distance ε is called the 'slip ratio' and is set to be 1% of the boundary-layer thickness δ, see Fig. 5.

At $r = 0$, P is finite. In Ref. [7] it is shown that at $r = \epsilon (\epsilon \ll 1)$ there is a coordinate singularity because $\mathrm{d}r \sim mP/\epsilon$. In Ref. [7] to avoid this singularity Eq. (3) is integrated from $r = \epsilon$. However, for high azimuthal mode orders, (large m), the numerical integration will be unstable because $P \sim 0$ in the centre of the duct where the flow is uniform.

Therefore, to calculate high mode orders it is proposed that for large m, the integration should start at $r = a$, and then $P(r)$ is matched to the solution for uniform flow at $r = a$, i.e. $P_{m,n}(r) = J_m(\kappa_{rm,n} r)$, $0 \leqslant r \leqslant a$. The choice of distance a will depend upon the azimuthal mode order m. The distance a is varied to ensure that the numerical integration of Eq. (3) remains stable. For high mode orders (m of the order of 100), $r = a$ may be some distance from the duct centreline at $r = 0$.

Having assumed the form of the solution in the region $0 \leqslant r \leqslant a$, it is straightforward to show that at $r = a$ the appropriate boundary condition is

$$\frac{\mathrm{d}p}{\mathrm{d}r} = f_a P, \tag{8}$$

where

$$f_a = \left(-\frac{m}{a} + \kappa_r \frac{J_{m-1}(\kappa_r a)}{J_m(\kappa_r a)} \right). \tag{9}$$

Then, a transfer matrix $\mathbf{T}$ is calculated, which relates P at $r = a$ and $r = b$ as follows:

$$\begin{bmatrix} P \\ \mathrm{d}P/\mathrm{d}r \end{bmatrix}_{r=b} = \begin{bmatrix} T_{11} & T_{12} \\ T_{21} & T_{22} \end{bmatrix} \begin{bmatrix} P \\ \mathrm{d}P/\mathrm{d}r \end{bmatrix}_{r=a}. \tag{10}$$

On substituting Eqs. (6) and (8) into Eq. (10), a non-trivial solution of Eq. (10) will be

$$F(k_z) = 0, \tag{11}$$

where

$$F = f_b T_{11} + f_a f_b T_{12} - T_{21} - f_a T_{22}. \tag{12}$$

The axial wavenumbers, k_z, of duct modes with a boundary-layer flow, are the roots of Eq. (11).

The transfer matrix $\mathbf{T}$ is constructed by integrating Eq. (3) using a fourth-order Runge–Kutta numerical integration scheme. Eq. (3) is expressed as two first-order equations in the form

$$\mathbf{x}' = \Lambda \mathbf{x}, \quad \mathbf{x} = \begin{bmatrix} P \\ \mathrm{d}P/\mathrm{d}r \end{bmatrix}. \tag{13}$$

The integration from $r = a$ to b is divided into N steps, with a variable step-size h which enables smaller increments to be used in the region close to the wall where there is a boundary layer. Then

$$\mathbf{T} = \mathbf{T}^N \mathbf{T}^{N-1} \ldots \mathbf{T}^2 \mathbf{T}^1, \tag{14}$$

where $\mathbf{T}^{l+1}$ (l is an integer) denotes the matrix such that

$$\mathbf{x}_{l+1} = \mathbf{T}^{l+1} \mathbf{x}_l, \tag{15}$$

and $\mathbf{T}^{l+1}$ is determined by setting $\mathbf{x}_l$ to be (1,0), and (0,1), and integrating Eq. (13) from $r = a + lh$ to $a + (l+1)h$.

The roots of Eq. (11), i.e. the axial wavenumbers k_z, can be found by using a complex root search routine. However, it is essential that the roots are located by using a systematic search routine because otherwise some modes may be missed.

With a boundary-layer flow, there are two additional points to consider. Firstly, with a uniform flow the vortical and acoustic perturbations are decoupled. Solutions of the convected Helmholtz equation are all acoustic. However, this is not true when there is a shear flow, and some of the solutions of Eq. (3) may be vortical (hydrodynamic) disturbances that are convected with the mean flow. Secondly, with a uniform flow in a lined duct there exist "surface" waves, see Refs. [10–12]. Tester [11] found that the axial wavenumber k_z for a surface wave mode can change significantly with the introduction of a boundary layer, even with a very thin shear layer. This will be problematic when searching for the k_z's with a boundary-layer flow, because the values of k_z for acoustic modes with a uniform flow would be ideal to use as initial guesses in a search routine.

A search method is now proposed that has been used to find the modes with a boundary-layer flow. Firstly, the modes with a uniform flow are calculated, see Refs. [2,3] and also Ref. [8]. In order to avoid the problem identified in Ref. [11], a linear shear profile with slip at the wall is introduced. Nayfeh et al. [13] have shown that the attenuation rate of modes in a lined flow duct with different boundary layer profiles tend to be comparable when the shape factors of each profile are equal.

The shape factor $H = \delta^*/\theta^*$, where δ^* and θ^* are the boundary layer's displacement and momentum thickness, respectively. For a linear shear profile with slip M_s at the wall,

$$H = \frac{3}{2(M_s/M_a) + 1}. \tag{16}$$

Note that for a uniform flow $M_s = M_a \Rightarrow H = 1$. For a 1/5th power law $H = 1.4$. (H is independent of the boundary-layer thickness.)

Firstly, taking a uniform flow, mode (m, n) is identified. Then, take a thin boundary layer which has a linear with slip profile. Starting from $M_s = M_a$, the slip at the wall is gradually reduced, and the change in the axial wavenumber $k_{zm,n}$ is tracked in the complex plane. Reducing the slip at the wall slowly increases H. The slip M_s is reduced until $H = 1.4$. The new value of $k_{zm,n}$ is then used as an initial guess to solve Eq. (11), for a 1/5th power law with the same thin boundary-layer thickness that was used with the linear with slip profile.

The use of a linear with slip profile avoids a sudden change in H when tracking $k_{zm,n}$. With small increments in M_s, it is possible to accurately track $k_{zm,n}$ in the complex plane. This provides a method to track the axial wavenumber $k_{zm,n}$ for mode (m, n), as a thin boundary layer is introduced into the flow. Having calculated $\mathrm{k}_{zm,n}$ for a thin 1/5th power law boundary-layer profile, the boundary-layer thickness is then slowly increased, and $k_{zm,n}$ is continued to be tracked in the complex plane, until the desired boundary-layer thickness is reached.

Tracking $k_{zm,n}$ in the complex plane should ensure, provided that the increments in the boundary-layer thickness are small, that the mode that is located also can be denoted mode '(m, n)'. This links this boundary-layer mode, with its corresponding Fourier–Bessel mode, i.e. compare Eqs. (2) and (1). Although this procedure can be quite laborious, it appears to work successfully at high frequencies. Results in this article have been calculated for modes at frequencies up to 10 BPF, i.e. kb between 250 and 300.

3. Results: boundary-layer "shielding"

The effect of boundary layer shielding on liner absorption is included in the modelling by utilizing the modal decay rates that are calculated by solving the Pridmore-Brown Eq. (3), following the procedure described in the previous section. Thus, these modified modal decay rates are only used for the lined inlet duct simulations. However, in addition to affecting the absorption in a lined duct, boundary layer shielding also could affect how the results of the comparison between measurement and prediction are interpreted.

In terms of duct modes, the rotor-alone pressure field is thought of in terms of a superposition of only first radial mode orders, because this means that owing to the shape of the first radial mode order eigenfunctions, the pressure is a maximum at or close to the duct wall.[4] The FDNS prediction method is based on a one-dimensional sawtooth pressure waveform that is used to approximate the rotor-alone pressure field. A Fourier decomposition of the waveform gives the pressure at each EO. This pressure is interpreted as the wall pressure. There is no radial dependence in the modelling, so taking the predicted pressure equivalent to the wall pressure relies on the assumption that the pressure is a maximum at or close to the duct wall.

In Ref. [4] it is postulated that, at high frequencies, boundary layer shielding could affect the wall measurements. If, owing to boundary layer shielding, the pressure is significantly higher outside the boundary layer, then the pressures predicted using the FDNS could be higher than the wall measurements, since the maximum pressure is in fact not at or close to the duct wall.

Therefore, in this section the effect of boundary layer shielding on sound absorption is examined, and also a brief comparison of mode eigenfunctions (with and without a boundary layer) is included to illustrate how boundary layer shielding could affect the wall measurements.

In Figs. 6–9 the predicted values of Δ_{LAM}, for rotor-alone EO modes with azimuthal mode order $m = \mathrm{EO} = 1$–$10B$, are shown for cases A, C, E and G. These figures are re-produced from Ref. [4], but now the attenuation with a boundary layer also has been included.

The predicted transmission losses are lower with a boundary layer, compared with a uniform mean-flow profile. Although at low supersonic fan speeds (e.g. case A, Fig. 6), the transmission losses at EOs in the liner's optimum frequency range are almost unchanged by the inclusion of a boundary layer. This is because at this low fan speed these modes are near cut-off. Therefore, the mode angles[5] will be close to 90°, so these modes are not refracted away from the duct wall by the boundary layer. In this case, the fan operating condition is the most significant factor. For example, a small change in the predicted value of the axial Mach number (M_a) would alter the modes' cut-off ratios, which would significantly affect the computed values of the modal decay rates.

The principal effect of a boundary layer is that the attenuation is predicted to be zero at high frequencies. This is because at high frequencies the rotor-alone modes are well cut-on. The direction of propagation of these modes is nearly parallel to the duct axis, i.e. mode angles close to 0°. Hence, these modes are completely shielded from the acoustic liner by the boundary layer, because only a small change in angle is necessary to refract these modes away from the duct wall. Regardless of the acoustic impedance of the liner, high-frequency sound will be shielded by the boundary layer, and not absorbed by the acoustic lining.

Figs. 6–9 also show examples of how the mode shapes change when a boundary layer is included in the mean-flow profile. At some mode orders, the least attenuated modes have radial order $n = 2$, owing to the presence of a surface wave. Tester [11] found that the introduction of a thin boundary layer can change the surface wave mode. This can be clearly seen in some of the examples in Figs. 6(c)–9(c). Notably at high fan

[4]The relative Mach number of the flow impinging on the fan blades is only supersonic near the duct wall, so the energy in the rotor-alone pressure field is localized close to the duct wall.

[5]Measured relative to the duct centreline at $\theta = 0°$.

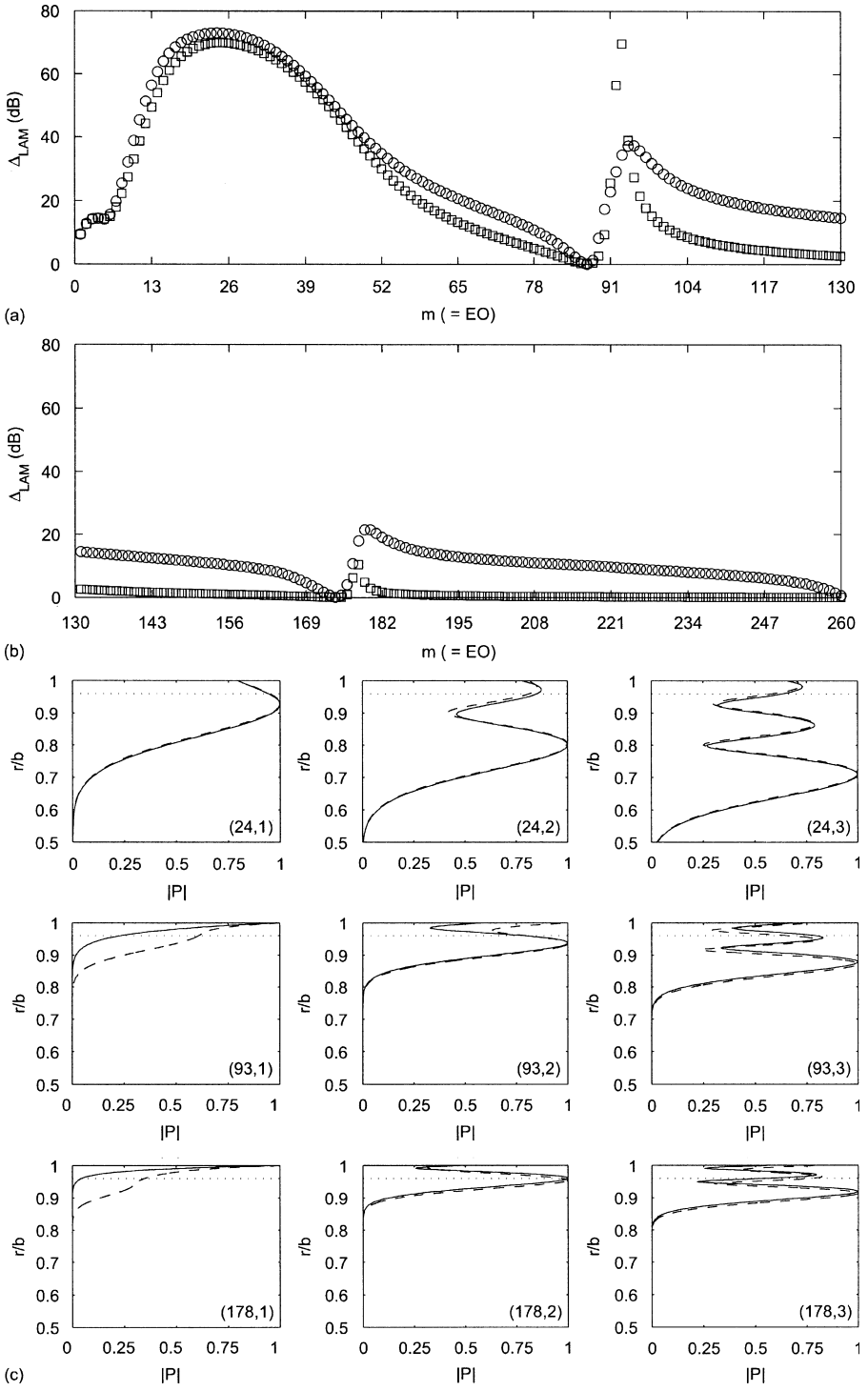

Fig. 6. Lined inlet duct—Case A. (a) Predicted attenuation of rotor-alone EO modes (○, uniform flow; □, boundary-layer flow). Δ_{LAM} for $m = EO = 1$ to $5B$, (b) Δ_{LAM} for $m = EO = 5B$ to $10B$. (c) Examples of predicted mode shapes (m, n) (—, uniform flow; - - -, boundary-layer flow). The boundary layer thickness is shown by the horizontal dotted line on each plot. Least attenuated modes: $m = 24$, $n = 1$; $m = 93$, $n = 2$; $m = 178$, $n = 2$.

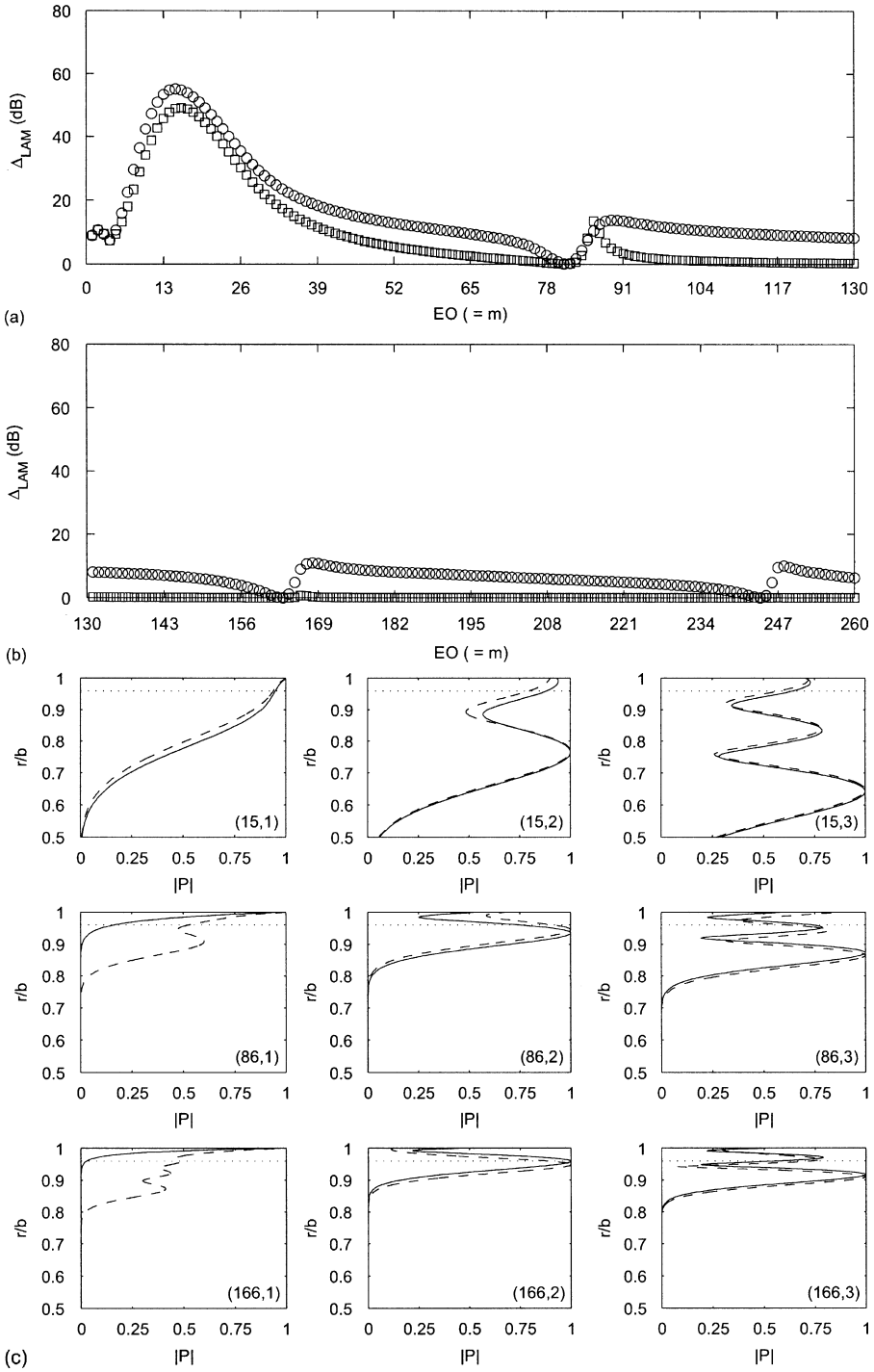

Fig. 7. Lined inlet duct—Case C. (a) Predicted attenuation of rotor-alone EO modes (○, uniform flow; □, boundary-layer flow). Δ_{LAM} for $m = EO = 1$ to $5B$, (b) Δ_{LAM} for $m = EO = 5B$ to $10B$. (c) Examples of predicted mode shapes (m, n) (—, uniform flow; - - -, boundary-layer flow). The boundary layer thickness is shown by the horizontal dotted line on each plot. Least attenuated modes: $m = 15$, $n = 1$; $m = 86$, $n = 2$; $m = 166$, $n = 2$.

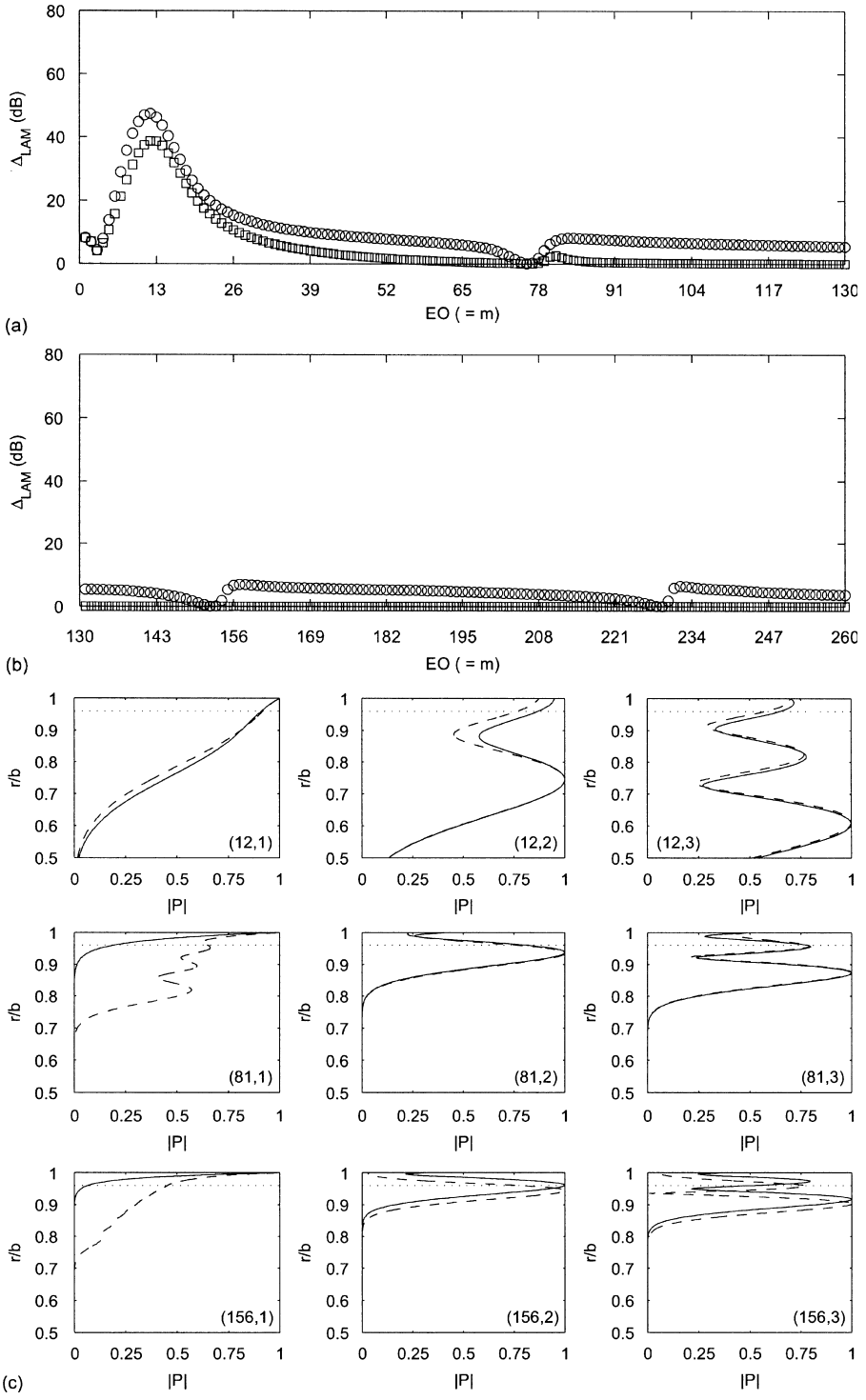

Fig. 8. Lined inlet duct—Case E. (a) Predicted attenuation of rotor-alone EO modes (○, uniform flow; □, boundary-layer flow). Δ_{LAM} for $m = EO = 1$ to 55, (b) Δ_{LAM} for $m = EO = 5B$ to $10B$. (c) Examples of predicted mode shapes (m, n) (—, uniform flow; - - -, boundary-layer flow). The boundary layer thickness is shown by the horizontal dotted line on each plot. Least attenuated modes: $m = 12$, $n = 1$; $m = 81$, $n = 2$; $m = 156$, $n = 2$.

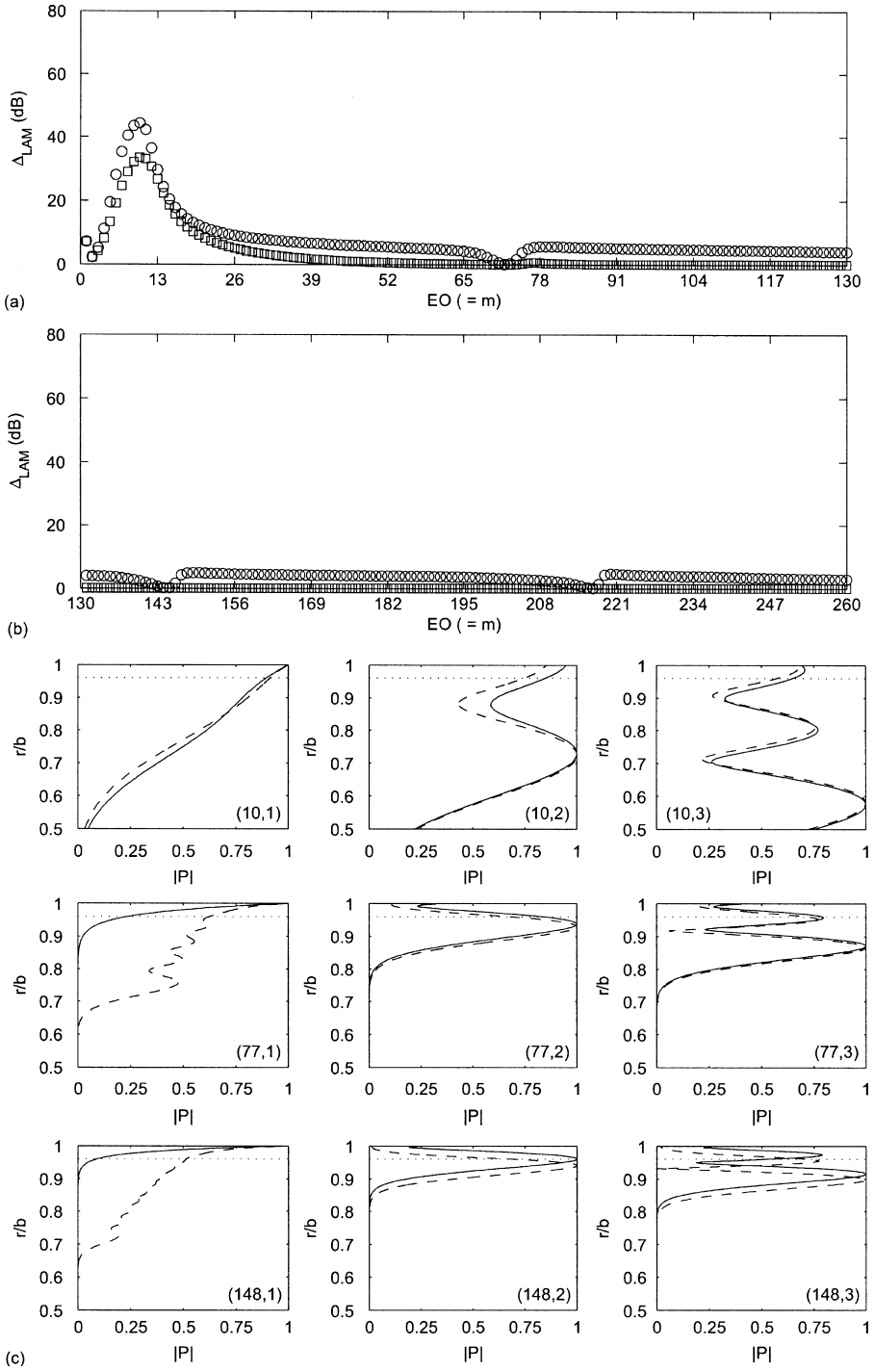

Fig. 9. Lined inlet duct—Case G. (a) Predicted attenuation of rotor-alone EO modes (○, uniform flow; □, boundary-layer flow). Δ_{LAM} for $m = EO = 1$ to $5B$, (b) Δ_{LAM} for m = EO = $5B$ to 105. (c) Examples of predicted mode shapes (m, n) (—, uniform flow; - - -, boundary-layer flow). The boundary layer thickness is shown by the horizontal dotted line on each plot. Least attenuated modes: $m = 10$, $n = 1$; $m = 77$, $n = 2$; $m = 148$, $n = 2$.

speeds, the introduction of the boundary layer has appreciably altered the surface wave's mode shape. The mode now appears to more closely resemble an instability (the mode does not decay evanescently with distance away from the wall). Further work is required to analyse these modes: however, in practice these modes are not the least attenuated modes (so are not included in the numerical simulations), and are likely only to be of some practical significance if they are unstable.[6]

The predicted transmission losses with a boundary layer have been used to re-calculate the FDNS numerical simulations reported in Ref. [4]. The updated predictions, for fan speed cases A–G, are shown in Fig. 10. There are two key features of these updated results to note.

It can be seen that the inclusion of a boundary layer leads to some improvement in the accuracy of the numerical simulations (compare Figs. 3 and 10). However, the improvement at frequencies in the liner's optimum frequency range is quite small, and generally the numerical simulations still under-predict the levels of the EO tones in this optimum frequency range. Also, at low supersonic fan speeds (case A, Fig. 10(a)) when the rotor-alone pressure field is near cut-off, it appears questionable whether reliable results can be obtained from these numerical simulations.

Now the inclusion of a boundary layer means it is predicted that there will be little or no attenuation at high frequencies. The inlet duct is effectively acoustically "hard" at high frequencies. This means at the high supersonic fan speeds there are small differences between the measured and predicted tone levels at high frequencies in both the rigid and lined ducts (compare Fig. 2(c),(d) with Fig. 10(e),(g)). The possible reasons for this discrepancy between the results have been discussed in Section 1. These explanations are not related to whether the duct wall is lined, so the updated simulations are more realistic because results for both the rigid and lined inlet duct, at high frequencies, are now more similar.

In Ref. [4] and here it is postulated that boundary-layer shielding could affect wall measurements at high frequencies. This effect is now briefly examined by comparing mode shapes with and without a boundary layer. Figs. 11 and 12 show examples of predicted mode shapes in a rigid duct at BPF and 4 BPF, i.e. rotor-alone EO modes (B, 1) and ($4B$, 1), respectively. In each figure the mode shapes, with and without a boundary layer, are compared for fan speed cases A, C, E and G. The boundary-layer thickness is 4% of the duct radius b.

At each fan speed, with no boundary layer the pressure maximum is located at the duct wall. The inclusion of a boundary layer alters the location of the pressure maximum, tending to shift the maximum inwards, closer to the edge of the boundary layer rather than the wall. At each fan speed the difference between this pressure maximum and the pressure at the wall is predicted to be higher at 4 BPF compared with BPF. As expected, the largest difference is at the highest fan speed, i.e. see Fig. 12(d). In this case the Helmholtz number $kb = 128.8$, and $k\delta = 5.2$, i.e. the acoustic wavelength and boundary-layer thickness are comparable lengths, and the pressure at the wall is predicted to be far lower than the pressure just outside the boundary layer.

These results illustrate how at high supersonic fan speeds, wall measurements at high frequencies could be affected by boundary-layer shielding. These examples are based only on the mean boundary-layer profile. In practice, it is not known how measurements by microphones at the duct wall are affected by the presence of a turbulent boundary layer. In order to determine quantitative estimates of boundary-layer shielding, that could be used to adjust wall measurements of high-frequency sound, a comparison between sound power determined by in-duct and far-field measurements is required. The far-field measurements would not be affected by the in-duct boundary layer.

In summary, the updated numerical simulations in an acoustically lined inlet duct show reasonably good agreement with the measured data, particularly at the higher fan speeds. However, the agreement at the low fan speeds remains poor, notably at case A. This is now examined with the aid of new modal measurements from a mode detection array. It is demonstrated that at low supersonic fan speeds, the assumption that buzz-saw noise is predominantly due to the rotor-alone EO tones is incorrect.

[6]There is one notable anomaly. At fan speed case A, the predicted attenuation at EO = 92–94 is higher when a boundary layer is included, compared with uniform flow, see Fig. 6(a). Here the least attenuated modes at these EOs have radial order $n = 2$, owing to the presence of a surface wave.

4. Results: modal measurements

The mode detection array was located near the end of the inlet duct, see Fig. 1. The array of non-equi-spaced microphones was able to resolve the modal spectrum up to about $m = 78$ (3 BPF). At each EO tone,

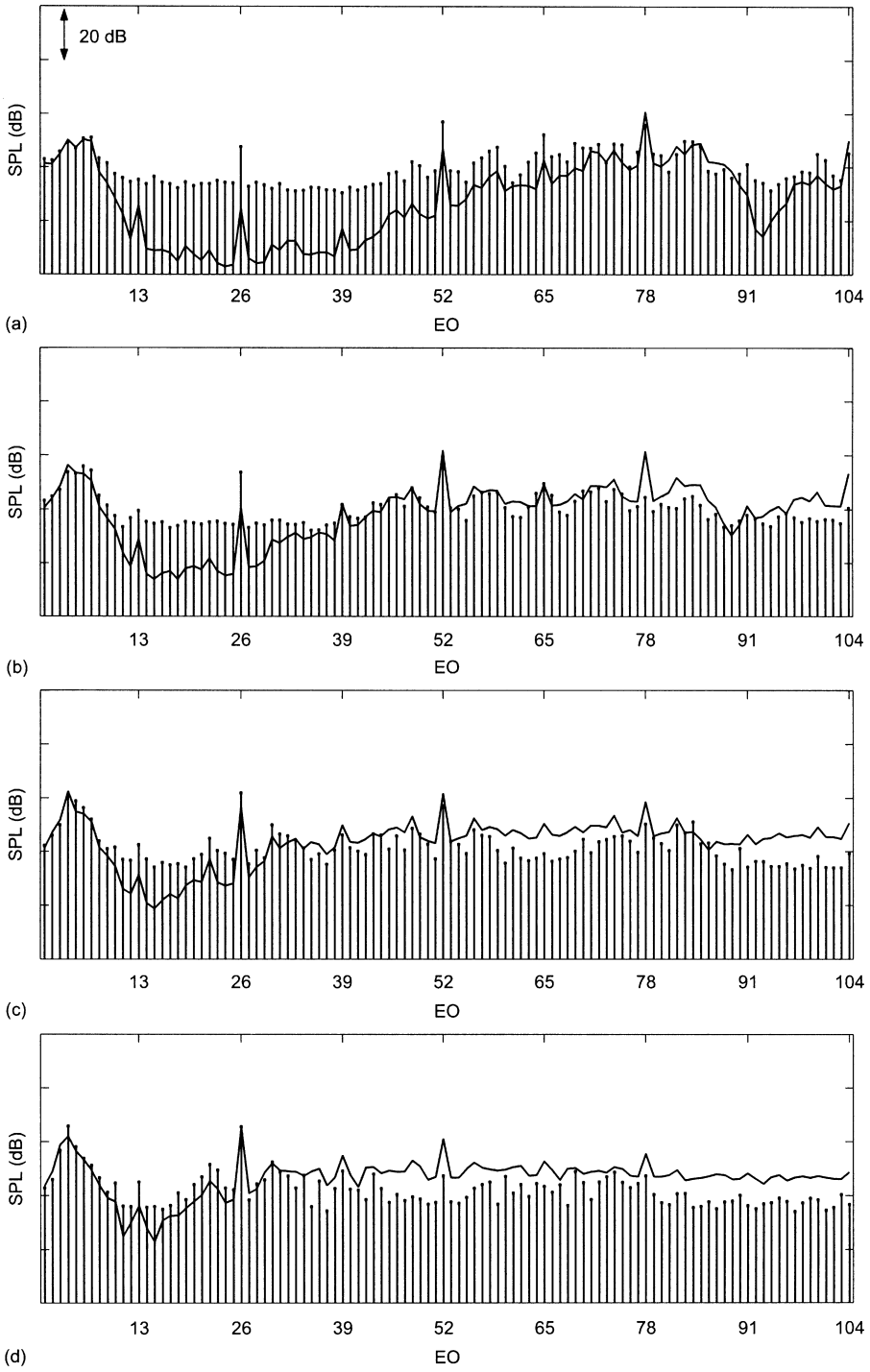

Fig. 10. Measured EO frequency spectrum at Kulite 4 in the lined inlet duct: (a) Case A; (b) Case B; (c) Case C; (d) Case D; (e) Case E; (f) Case F; and (g) Case G. The improved FDNS prediction is shown by solid line (boundary-layer thickness 4%).

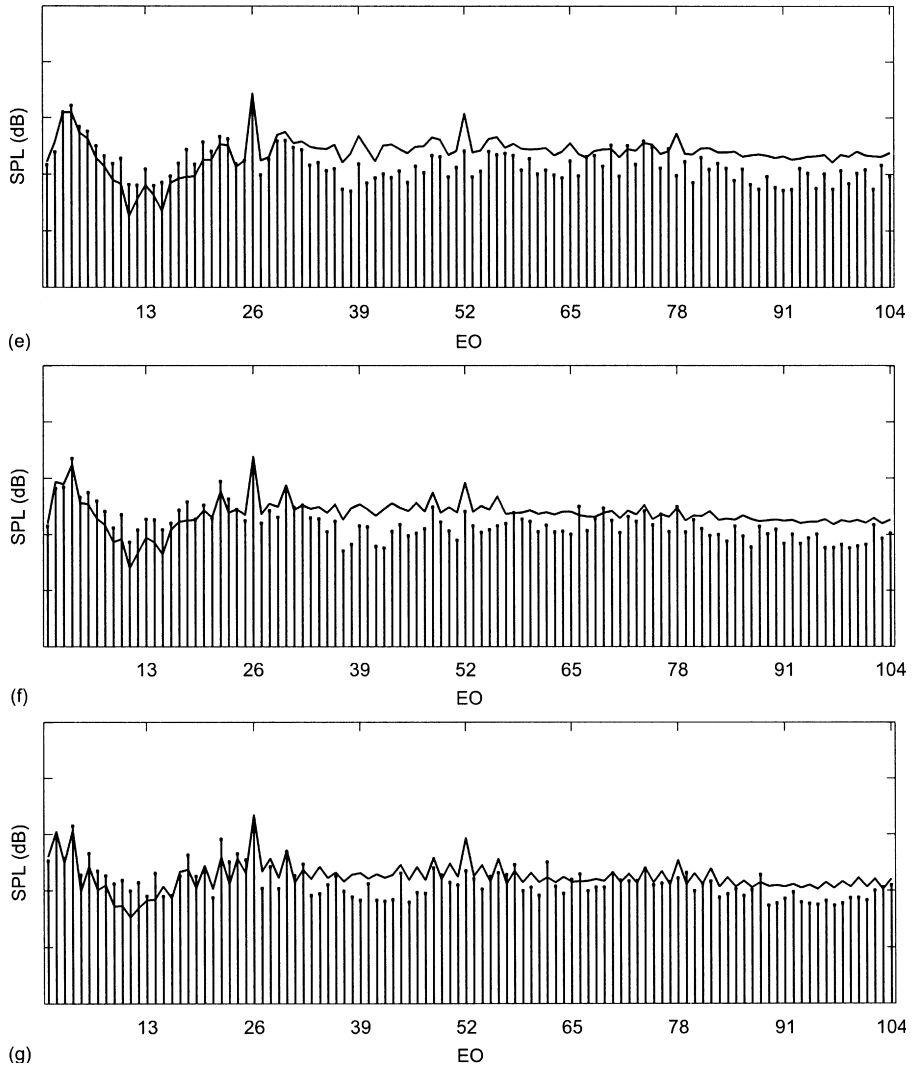

Fig. 10. (*Continued*)

different modes were identified based on their azimuthal mode order. For each EO tone, the rotor-alone and non-rotor-alone modes can be distinguished because the former have $m = \text{EO}$, whilst the latter have $m \neq \text{EO}$.

Two examples of measurements obtained from the mode detection array are included in this article (some of these measurements are also in Ref. [5]). Firstly, at a fixed frequency, the measured SPL is compared against the level of the rotor-alone component of the tone, for fan speeds in the range $0.9 \leqslant M_t \leqslant 1.3$ (M_t is the rotor blade tip Mach number). Results at $\frac{1}{2}$BPF, BPF, $\frac{3}{2}$BPF and 2 BPF, i.e. EOs $\frac{1}{2}B$, B, $\frac{3}{2}B$ and $2B$, are shown in Figs. 13–16. Secondly, the EO frequency spectrum (up to EO $= 3B = 78$), at fan speed cases A, C, E and G is shown in Fig. 17. At each fan speed, the measured SPL is compared against the rotor-alone $m = \text{EO}$ component of the tones. Also shown in Figs. 13–17 are results from the numerical simulations.

In Ref. [5] the azimuthal mode breakdown of the BPF tone is examined in detail. The two principal sources of non-rotor-alone modes are "liner scattered" and "distortion" tones. These tonal sources are similar to the well-known rotor–stator interaction tones identified originally by Tyler and Sofrin [14].[7] The fan case liner had

[7]In Ref. [14] it is demonstrated that the interaction of rotating fan blade wakes and fixed stator vanes leads to tones with mode number $m = lB \pm jV$, where B is the number of fan blades, V the number of stator vanes, and l, j are integers.

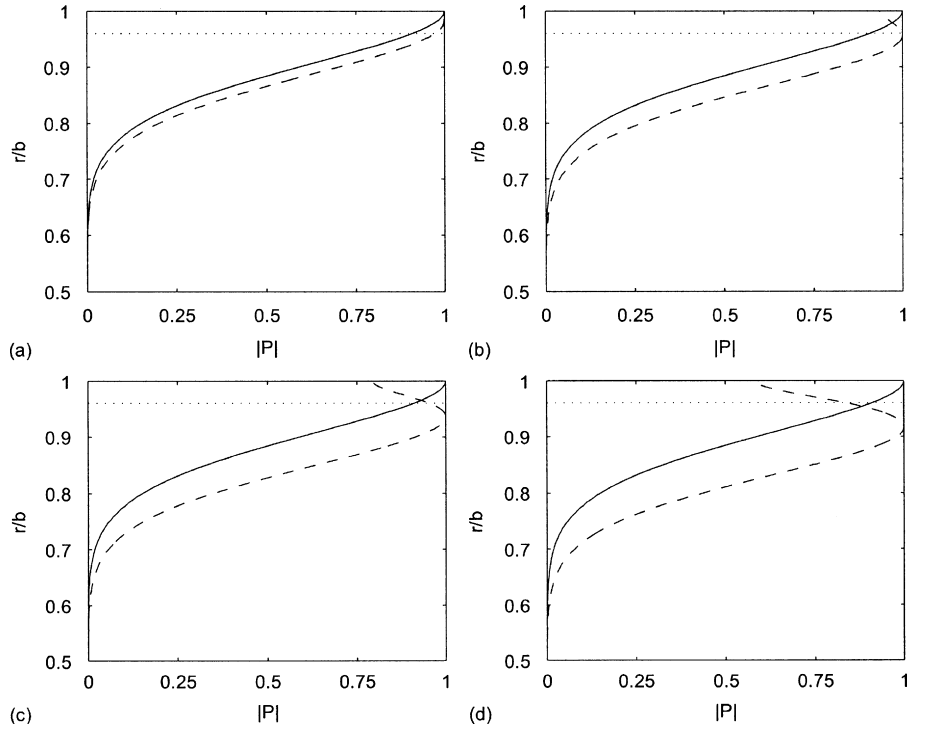

Fig. 11. Examples of predicted mode shapes in a rigid duct at BPF (—, uniform flow; - - -, boundary-layer flow). Rotor-alone EO mode (B, 1): (a) Case A; (b) Case C; (c) Case E; and (d) Case G. The boundary layer thickness is shown by the horizontal dotted line on each plot.

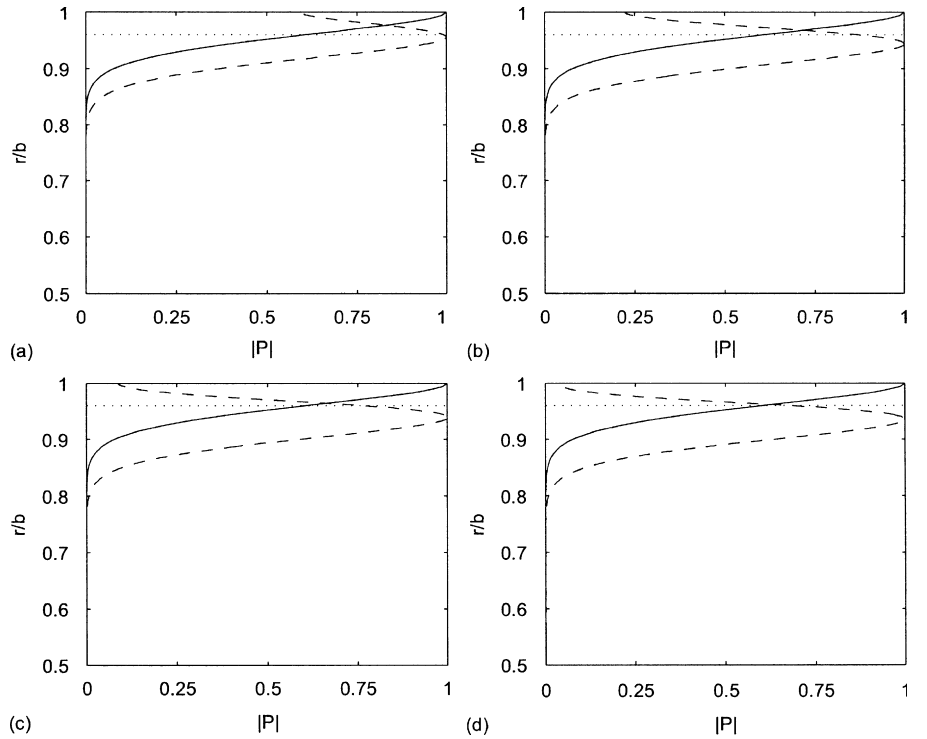

Fig. 12. Examples of predicted mode shapes in a rigid duct at 4BPF (—, uniform flow; - - -, boundary-layer flow). Rotor-alone EO mode ($4B$, 1): (a) Case A; (b) Case C; (c) Case E; and (d) Case G. The boundary layer thickness is shown by the horizontal dotted line on each plot.

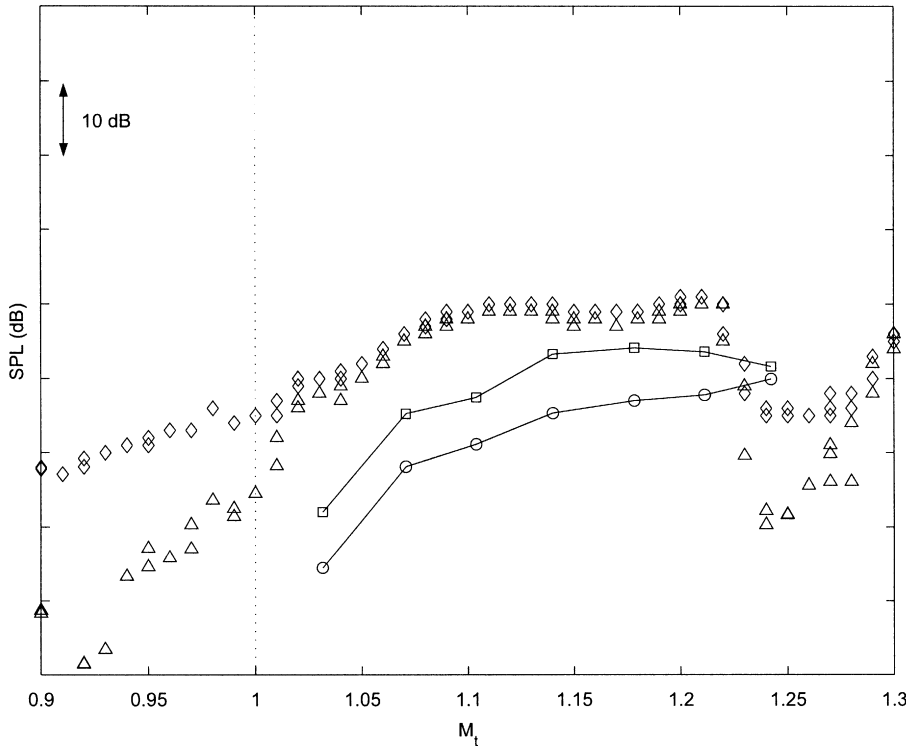

Fig. 13. Comparison between measurement by mode detection array (MDA) and prediction. Frequency $= \frac{1}{2}$BPF. MDA: $\diamond$, EO $= \frac{1}{2}B$; Δ, $m = \frac{1}{2}B$. FDNS: $\square$, boundary-layer thickness 4%; $\circ$, uniform flow. $M_t = 1$ is shown by the vertical dotted line.

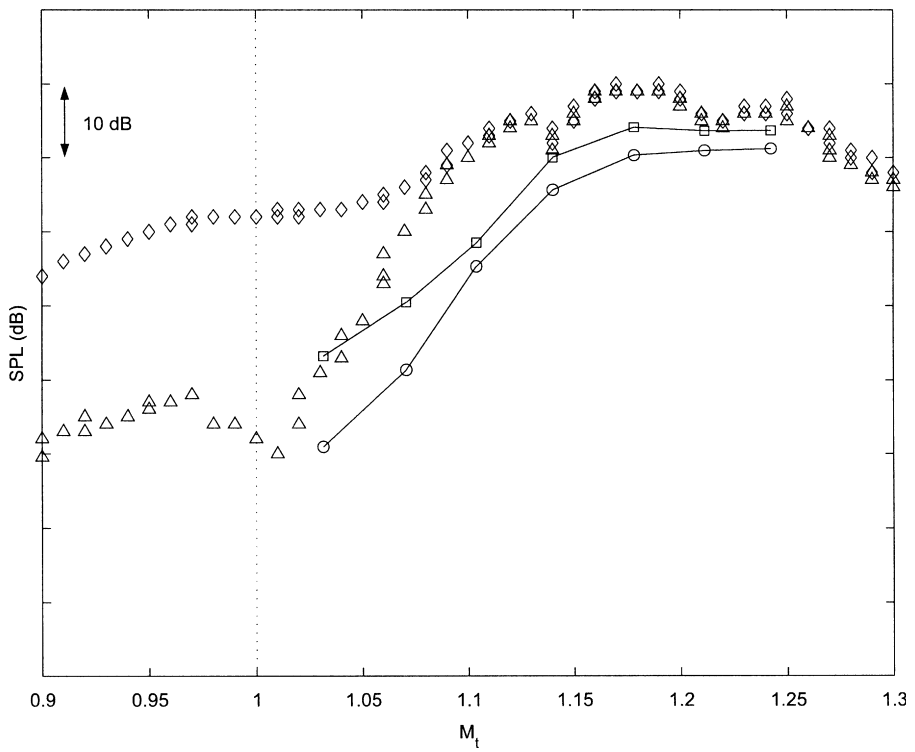

Fig. 14. Comparison between measurement by mode detection array (MDA) and prediction. Frequency = BPF. MDA: $\diamond$,EO $= B$; Δ,$m = B$. FDNS: $\square$, boundary-layer thickness 4%; $\circ$, uniform flow. $M_t = 1$ is shown by the vertical dotted line.

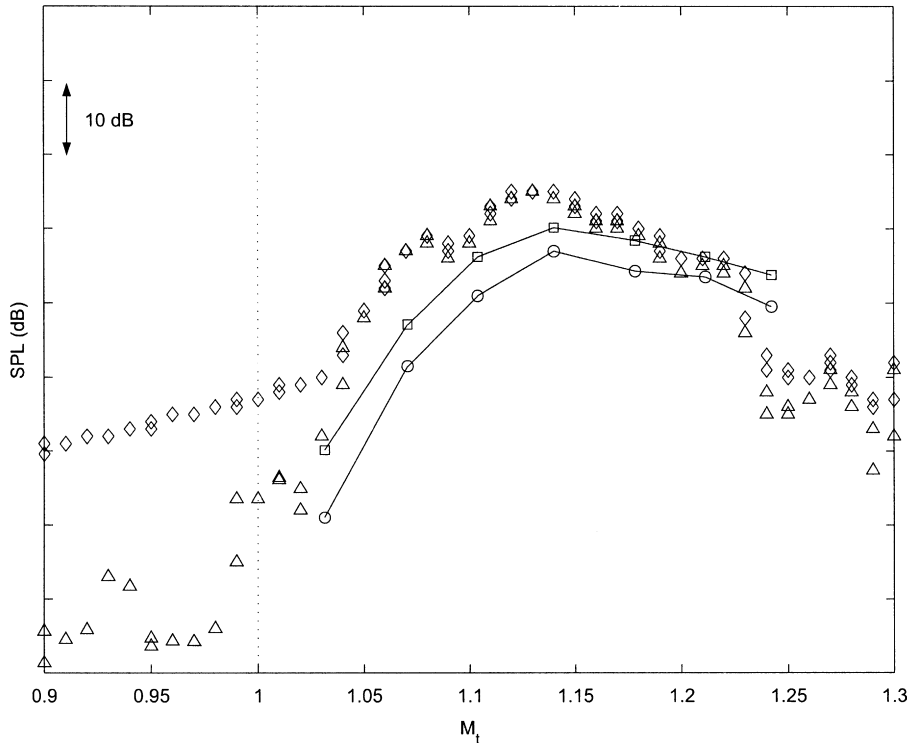

Fig. 15. Comparison between measurement by mode detection array (MDA) and prediction. Frequency $= \frac{3}{2}$BPF. MDA: $\diamond$, EO $= \frac{3}{2}B$; Δ, $m = \frac{3}{2}B$. FDNS: $\square$, boundary-layer thickness 4%; $\circ$, uniform flow. $M_t = 1$ is shown by the vertical dotted line.

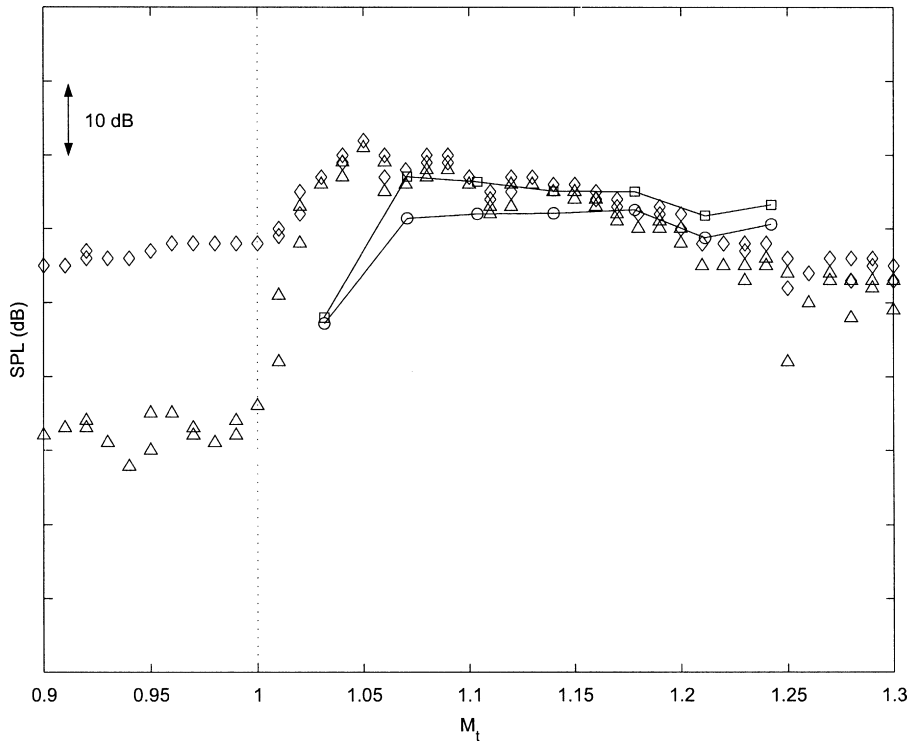

Fig. 16. Comparison between measurement by mode detection array (MDA) and prediction. Frequency $= 2$ BPF. MDA: $\diamond$, EO $= 2B$; Δ, $m = 2B$. FDNS: $\square$, boundary-layer thickness 4%; $\circ$, uniform flow. $M_t = 1$ is shown by the vertical dotted line.

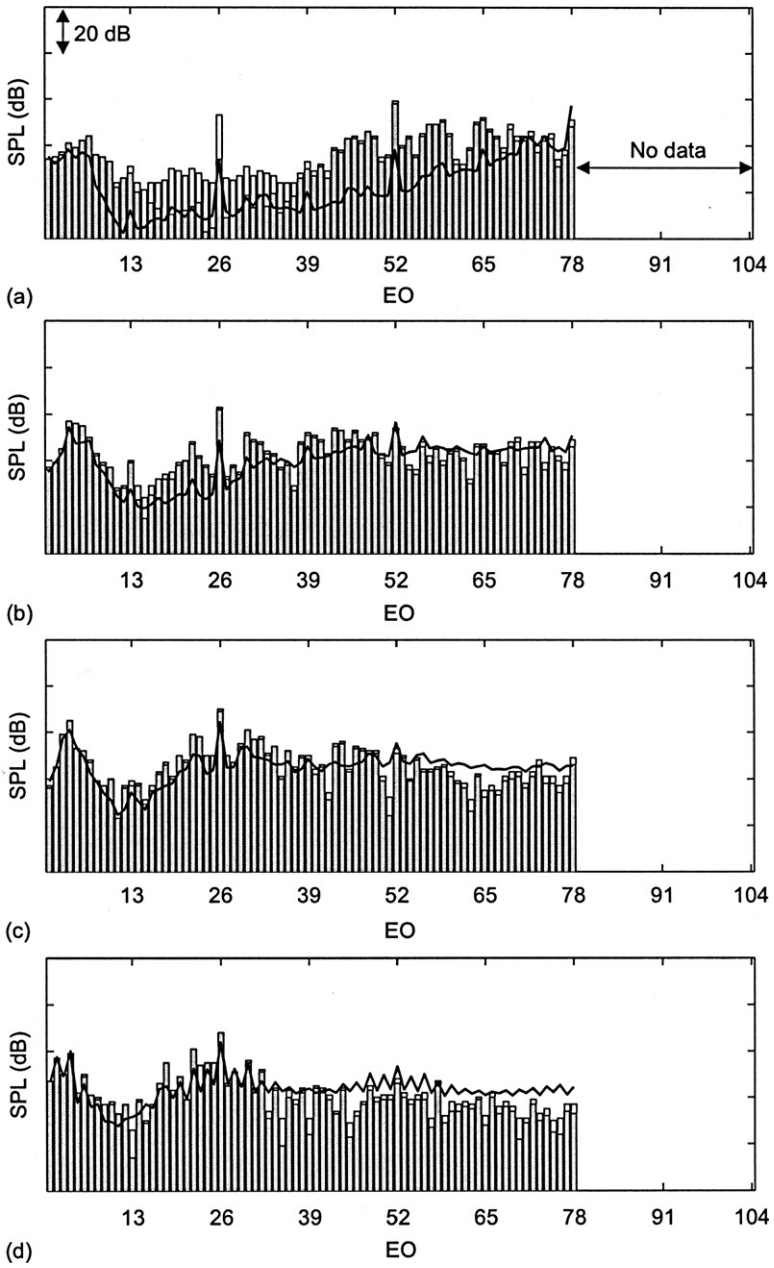

Fig. 17. Comparison between measurement by mode detection array (MDA) and prediction. EO frequency spectrum EO = 1 to 3B: (a) Case A; (b) Case C; (c) Case E; and (d) Case G. MDA: white bars, EO tone level; grey bars, m = EO only. The improved FDNS prediction is shown by solid line (boundary-layer thickness 4%).

eight longitudinal hard splices which can generate acoustic scattering. In Ref. [5] (see Fig. 11, p. 10) liner scattered modes with $m = B-8$, $B-16$, $B-24$ are identified, due to scattering by the 8 liner splices. Also, the inlet flow contained distortion, i.e. the mean flow varied around the duct circumference, owing to the slight asymmetry of the inlet. Mean-flow distortion is typically of low order. Also in Ref. [5] a distortion mode with $m = B-1$ is identified, due to a mean-flow distortion with azimuthal order $m = 1$. The non-rotor-alone scattered modes were detected over the entire supersonic fan speed range, but it is only at low supersonic fan speeds that the amplitude of some of these modes exceeds the amplitude of the rotor-alone modes.

At low supersonic fan speeds, the BPF mode $m = B$ is near cut-off, and is predicted to be well absorbed by the acoustic lining. As shown in [5], energy from the BPF tone is scattered into non-rotor-alone modes because of the presence of liner splices and mean-flow distortion. Some of these modes ($m < B$) rotate with a faster circumferential phase speed than the fan, and are less near cut-off, compared with the BPF mode $m = B$. Consequently, these scattered modes will be less well absorbed by the lining, and by the end of the inlet duct, these modes may be the dominant noise source at BPF. The scattered modes only will be significant if the rotor-alone modes are well absorbed by the acoustic lining, whilst the scattered modes are not. This only will occur at low supersonic fan speeds, when the rotor-alone pressure field is near cut-off, and at frequencies in the liner's optimum frequency range.

The assumption that the numerical simulation method, FDNS, can be used for buzz-saw noise predictions is based on the assumption that the principal source of buzz-saw noise are the rotor-alone EO tones. The simulations only predict the level of the rotor-alone tones. The numerical results are now re-examined, in light of modal measurements from the mode detection array.

The speed range shown in Figs. 13–16 includes fan speeds in excess of 90%, $M_t > 1.2$. The measured levels tend to fall at very high speeds as the fan speed approaches design, due to the onset of shock swallowing. The numerical method appears practical to use at supersonic fan speeds up to about 90%.

At $\frac{1}{2}$ BPF (see Fig. 13), the measured levels of the EO tone and the rotor-alone EO tone are approximately the same, apart from when the rotor-alone pressure field is near cut-off (as $M_t \to 1$). This means that the source of the buzz-saw noise is the rotor-alone EO tone. The improved numerical simulations (boundary-layer included) consistently predict the level of the rotor-alone tone to be about 10 dB less than is measured. It is noted that $\frac{1}{2}$ BPF is generally within the liner's optimum frequency range, so the predicted modal decay rates used in the numerical simulations are high, with or without a boundary layer included in the modelling.

At 1 BPF (see Fig. 14), the measured levels of the EO tone and the rotor-alone EO tone are approximately the same when $M_t > 1.1$. However, at lower supersonic fan speeds, the rotor-alone EO tone level falls sharply, such that by $M_t = 1$ the rotor-alone component of the BPF tone is about 30 dB less than the measured SPL at BPF. In this speed range, $1 < M_t < 1.1$, the rotor-alone tone is *not* the dominant source of buzz-saw noise. The improved numerical simulations show much better agreement with the measurements when compared against the rotor-alone component of the BPF tone, as opposed to the measured SPL. Although again the simulations consistently under-predict the level of the rotor-alone tone, these modal measurements demonstrate why large discrepancies between the measured and predicted tone levels, of the order of 20–30 dB, have been seen at low fan speeds, notably at case A.

At $\frac{3}{2}$ and 2 BPF (see Figs. 15 and 16), the measured levels of the EO tone and the rotor-alone EO tone also are approximately the same. The improved numerical simulations show reasonable agreement with the measured tones, although at 2 BPF it appears that the curve showing the predicted level of the tone needs to be shifted slightly to the left to better fit the data.

In Fig. 17, the numerical simulations also are compared against the EO frequency spectrum, measured by the mode detection array, at fan speed cases A, C, E and G. The measurements include both the SPL of each EO tone, and the SPL of the rotor-alone $m =$ EO component of the spectrum. For example, see the EO frequency spectrum at fan speed case A shown in Fig. 17(a); in the frequency range from about $\frac{1}{2}$ to $\frac{3}{2}$ BPF the EO frequency spectrum is not dominated by the rotor-alone $m =$ EO modes. In fact, in this frequency range there is reasonably close agreement between the simulation and the $m =$ EO spectrum, although the comparison is still poor at other frequencies, notably at frequencies greater than $\frac{3}{2}$ BPF.

It appears that the difference between the measured and predicted results at low fan speeds can be partly explained by the modal measurements. However, clearly the predicted modal decay rates at this fan speed are higher than the measured attenuation. This is presumably because as M_t approaches 1 *all* the rotor-alone tones become cut-off, so the validity of the simulations at supersonic fan speeds close to the sonic point, $M_t = 1$, is questionable because the rotor-alone pressure field is near cut-off.

At fan speed cases C, E and G, the SPL EO frequency spectrum and the $m =$ EO spectrum are approximately the same. The improved numerical simulations show good agreement with the measurements, in particular at fan speed cases E and G, see Fig. 17(c, d).

5. Conclusions

The numerical simulations are an engineering method to use for buzz-saw noise predictions. The numerical method had been developed previously, see Refs. [2,3], but until now had not been fully benchmarked by comparison with experimental measurements.

The method is not based on computational fluid dynamics, which is difficult to apply to buzz-saw noise because of the complexity of the problem. Instead, a simple approach based on a one-dimensional approximation of the rotor-alone pressure field in a turbofan inlet duct is used. The principal feature of the method is that, to a first approximation, absorption of sound by an acoustic lining is modelled. In this article, an improved prediction method is proposed which utilizes modal decay rates in a lined duct containing a shear flow with a thin boundary layer at the duct wall.

The inclusion of a boundary layer in the mean-flow profile provides a more realistic model of the absorption of sound in a lined duct. With a boundary layer, the predicted modal decay rates of the rotor-alone EO modes are less than the predicted decay rates with a uniform flow. In particular, at high frequencies the sound is almost completely refracted, or shielded, from the duct wall by the boundary layer. Consequently, at high frequencies the duct wall is acoustically hard.

Using the modal decay rates calculated with a boundary-layer flow leads to some improvement in the comparison of measurement with prediction, but there remains some frequencies at which the agreement is relatively poor. This is typically at EOs in the liner's optimum frequency range. At these frequencies the transmission losses are predicted to be high, but based on the measured data, it appears that the attenuation is generally less than is predicted.

A more realistic estimate of the transmission losses in a lined inlet duct would be useful. Currently, these losses are predicted based on a uniform circular-section duct that contains a uniform mean flow with a thin boundary layer at the wall. In practice, the duct geometry and mean flow are not uniform, and one area for future work is whether a more realistic model of the inlet duct is necessary, to better predict the attenuation in a lined inlet. It is difficult to assess the accuracy of the estimates of the specific acoustic impedance of the liner in the presence of flow and high SPLs.

Also, the modal decay rates are highly dependent on cut-off ratio, particularly modes near cut-off. The accuracy of numerical simulations at low supersonic fan speeds are particularly affected by the sensitive nature of cut-off, because high theoretical decay rates may not be that realistic as M_t decreases (i.e. as $M_t \rightarrow 1$). However, at low supersonic fan speeds it has also been demonstrated that the source of buzz-saw noise is not only the rotor-alone EO tones.

Modal measurements have been examined to investigate acoustic scattering, and its affect on buzz-saw noise. The mode detection results demonstrate that at low supersonic fan speeds, when the rotor-alone pressure field is near cut-off, the levels of some scattered modes are higher than the rotor-alone EO modes.

It has been shown that the FDNS numerical simulations generate realistic predictions of the type of buzz-saw EO frequency spectrum that is measured in turbofan rigid and lined inlet ducts. The prediction method only can be used to predict the rotor-alone pressure field. Therefore, it may not be suitable to use for buzz-saw noise predictions at low supersonic fan speeds, close to the sonic point $M_t = 1$, when the rotor-alone pressure field is near cut-off. Also, at high supersonic fan speeds, close to the fan's design speed, it may not be suitable because the one-dimensional approximation that is used to model the rotor-alone pressure field is not realistic.

In order to reconstruct the pressure field exactly, amplitude *and* phase measurements are required. Until now only spectral measurements were available, but recently measurements of both amplitude and phase have been obtained. Future planned work will use these measurements to examine the rotor-alone pressure field, in addition to the EO frequency spectrum. Also, it is anticipated that comparison with full CFD solutions will be possible soon.

Acknowledgements

The authors wish to warmly acknowledge Drs. E. R. Rademaker and P. Sijtsma (National Aerospace Laboratory NLR, The Netherlands) for their work on the mode detection array that was used during the

Rolls–Royce RESOUND fan rig test. Additional data that was not in Ref. [5], obtained during the RESOUND experimental tests with the mode detection array, has been included in this article.

The work was funded by the European Community X-noise research projects RESOUND and DUCAT. The support of Mr. P. Kruppa (Technical Monitor for the Commission) is particularly acknowledged.

AM and MJF wish to acknowledge the continuing financial support provided by Rolls–Royce plc.

References

[1] M.J. Fisher, B.J. Tester, P.J.G. Schwaller, Supersonic fan tone noise prediction, AIAA 98–2249, 1998.
[2] A. McAlpine, M.J. Fisher, On the prediction of "buzz-saw" noise in aero-engine inlet ducts, *Journal of Sound and Vibration* 248 (1) (2001) 123–149.
[3] A. McAlpine, M.J. Fisher, On the prediction of "buzz-saw" noise in acoustically lined aeroengine inlet ducts, *Journal of Sound and Vibration* 265 (1) (2003) 175–200.
[4] A. McAlpine, M.J. Fisher, B.J. Tester, "Buzz-saw" noise: A comparison of measurement with prediction, *Journal of Sound and Vibration* 290 (2006) 1202–1233.
[5] E.R. Rademaker, P. Sijtsma, B.J. Tester, Mode detection with an optimised array in a model turbofan engine intake at varying shaft speeds, AIAA 2001–2181, 2001.
[6] P. Mungur, H.E. Plumblee, Propagation and attenuation of sound in a soft-walled annular duct containing a sheared flow, NASA SP-207, 1969, pp. 305–327.
[7] W. Eversman, Effect of boundary layer on the transmission and attenuation of sound in an acoustically treated circular duct, *Journal of the Acoustical Society of America* 49 (1971) 1372–1380.
[8] W. Eversman, Theoretical models for duct acoustic propagation and radiation, in: H.H. Hubbard (Ed.), *Aeroacoustics of Flight Vehicles: Theory and Practice, Vol. 2. Noise Control*, NASA RP-1258, 1991, pp. 101–163.
[9] D.C. Pridmore-Brown, Sound propagation in a fluid flowing through an attenuating duct, *Journal of Fluid Mechanics* 4 (1958) 393–406.
[10] B.J. Tester, The propagation and attenuation of sound in lined ducts containing uniform or "plug" flow, *Journal of Sound and Vibration* 28 (2) (1973) 151–203.
[11] B.J. Tester, Some aspects of "sound" attenuation in lined ducts containing inviscid mean flow with boundary layers, *Journal of Sound and Vibration* 28 (2) (1973) 217–245.
[12] S.W. Rienstra, A classification of duct modes based on surface waves, *Wave Motion* 1107 (2002) 1–17.
[13] A.H. Nayfeh, J.E. Kaiser, B.S. Shaker, Effect of mean-velocity profile shapes on sound transmission through two-dimensional ducts, *Journal of Sound and Vibration* 34 (1974) 413–423.
[14] J.M. Tyler, T.G. Sofrin, Axial flow compressor noise studies, *SAE Transactions* 70 (1962) 309–332.